The Cryosphere Discuss., 7, 921–941, 2013
www.the-cryosphere-discuss.net/7/921/2013/
doi:10.5194/tcd-7-921-2013

The Cryosphere Discussions
Open Access

A particle based simulation model for glacier dynamics

J. A. Åström[1], T. I. Riikilä[2], T. Tallinen[2], T. Zwinger[1], D. Benn[3,4], J. C. Moore[5,6,7], and J. Timonen[2]

[1]CSC – It-centre for science, P.O. Box 405, 02101, Esbo, Finland
[2]Department of Physics, University of Jyväskylä, P.O. Box 35 (YFL), 40014, Jyväskylä, Finland
[3]Department of Geology, University Centre in Svalbard, 9171 Longyearbyen, Norway
[4]School of Geography and Geosciences, University of St Andrews, Fife, KY16 8ST, UK
[5]State Key Laboratory of Earth Surface Processes and Resource Ecology, College of Global Change and Earth System Science, Beijing Normal University, Beijing, China
[6]Arctic Centre, University of Lapland, PL122, 96100 Rovaniemi, Finland
[7]Department of Earth Sciences, Uppsala University, Villavägen 16, Uppsala, 75236, Sweden

Received: 29 January 2013 – Accepted: 4 February 2013 – Published: 6 March 2013

Correspondence to: J. A. Åström (jan.astrom@csc.fi)

Published by Copernicus Publications on behalf of the European Geosciences Union.

Abstract

A particle-based computer simulation model was developed for investigating the dynamics of glaciers. In the current model, large ice bodies are made of discrete elastic particles which are bound together by massless and elastic beams. The beams can break which induces brittle behaviour. At loads below fracture, beams may also break and reform with small probabilities in order to incorporate slowly deforming viscous behaviour in the model. This model has the advantage that it can simulate important physical processes such as ice calving and fracturing in a more realistic way than traditional continuum models. Two simulations were performed: (1) calving of an ice block partially supported in water, which could represent a grounded marine glacier terminus, and (2) fracturing of an ice block on an inclined plane of varying basal friction, which could represent transition to fast flow or surging. For benchmarking purposes the deformation of an ice block on a slip-free surface was compared to that of a similar block simulated with a Finite Element full-Stokes continuum model. In spite of several simplifications, which include restriction to two-dimenions and simplified rheology for water, the model introduced was able to reproduce the size distributions of the icebergs and the debris observed in calving. The size distributions we produce may be approximated by universal scaling laws. On a moderate slope, a large ice block was stable as long as there was enough of friction against the substrate. This was a quiescent state. For a critical length of frictional contact global sliding began, and the model block disintegrated in a manner suggestive of a surging glacier. In this case the fragment size distribution produced was typical of a grinding process.

1 Introduction

The formation and propagation of fractures underpins a wide range of important glaciological processes including crevasse formation, iceberg calving and rheological weakening of ice in shear margins and icefalls. Numerical simulations of glaciers, however, almost exclusively employ continuum methods which treat ice as a continuous medium with uniform or smoothly varying properties. The difficulty of dealing with discontinuities in continuum models means that the effects of fracturing are routinely represented by simple parameters, such as depth of fracture penetration (Benn et al., 2007a,b; Nick et al., 2010), bulk "damage" (Jouvet et al., 2011; Borstad et al., 2012), or ice softness (Vieli et al., 2006). While useful for many purposes, these approaches impose major limitations on the kinds of glacier behaviour that can be represented in prognostic models.

Glacier fracture and iceberg calving have been relatively little studied, perhaps because of the statistical nature of the work requires long term monitoring. In the regions where it has been documented, however, calving constitutes up to 40–50 % of mass loss on marine terminating ice fronts (Burgess et al., 2005; Dowdeswell et al., 2008; Walter et al., 2010; Thomas et al., 2004). Marine terminating glaciers account for almost all mass loss through calving in the case of Antarctica and about 50 % for Greenland (Rignot et al., 2011; Jacob et al., 2012). Calving glaciers are very variable, but two end member types can be recognized: (i) glaciers with grounded termini, and (ii) floating ice shelves that are constrained only at their lateral margins. The two scenarios produce radically different types of calving: (i) small ice blocks that fall off the calving cliff in typically warm tidewater glacier settings, and (ii) large flat-topped bergs that can be tens of km across from the colder ice shelves that fringe the polar ice sheets. At present no ice sheet model incorporates calving as a function of atmospheric and oceanic forcing. Indeed, no formulation for calving has yet been agreed as suitable for models, though several have been proposed (Benn et al., 2007a; Nick et al., 2010; Bassis, 2011; Levermann et al., 2012), and indeed different ones may be suitable for different applications such as large scale models (e.g. Levermann et al., 2012) or basin-scale studies (Benn et al., 2007a) with floating ice tongues (e.g. Nick et al., 2010).

Benn et al. (2007a) proposed a physically based model with the position of the calving front depending on the depth of penetration of surface crevasses, which in turn

TCD
7, 921–941, 2013

depends on the longitudinal strain rate. A modification suggested was to increase crevasse depth by the filling of crevasses by surface melt water, which is common occurrence in summer even on ice sheets, and certainly typical of many marine terminating smaller glaciers. Nick et al. (2010) introduced a further modification by including basal crevasses with a calving criterion when surface crevasses reach basal crevasses. Basal crevasses can penetrate much farther than surface air-filled crevasses, hence potentially triggering calving at a greater distance from the terminus. The existence of huge tabular icebergs, originating from floating ice shelves, provides ample motivation for incorporating this effect.

In this paper, we introduce a new, particle-based method for modeling ice flow, which allows elastic, viscous and brittle behaviour to be represented within a single framework. Although based on simple rules, a very wide range of glaciological phenomena emerge from the model, allowing detailed investigation of processes that are difficult or impossible to represent in continuum models. We first describe the model, then illustrate some of its potential applications, including calving events, the effects of variable basal friction, and threshold behavior in sliding rates ("surging"). We also present an ice-deformation calculation using the particle code and the FEM code Elmer/Ice (http://elmerice.elmerfem.org) for benchmarking.

2 Model

In our simulation model, a large ice-body is divided into discrete circular particles. The typical diameter of the particles is in the present simulations of the order of 1 m. Initially, at the start of a simulation, such particles are densely packed to form a large body, and the particles are assumed to be frozen together. The particles can either be arranged more or less randomly as in an amorphous solid, or as in a regular lattice. The frozen contacts between the particles are modelled by elastic massless beams which can break if stretched or bent beyond a threshold limit. In such a case the beam vanishes (see Fig. 1). No mass is lost in this process. If particles detach, they are able to flow

TCD
7, 921–941, 2013

past each other and thereby collide with other particles. The detailed deformation of the particles is not modelled. The contact forces in a collision are calculated as function of minute ovelapping of particles. The collisions are inelastic and kinetic energy is lost in every collision. This means that once all contacts are broken and the ice-block is under local compression, the ice will display granular flow. For unbroken parts the ice will continue to behave as an elastic solid. Under tension the ice is able to fracture via crack formation and propagation. The model should thus contain all the necessary ingredients for simulating ice dynamics, at least on a qualitative level. The equations of motion are given by:

$$\mathbf{M}\ddot{\boldsymbol{r}}_i + \mathbf{C}\dot{\boldsymbol{r}}_i + \gamma_{ij}\mathbf{C}'\dot{\boldsymbol{r}}_{ij} + \gamma'_{ij}\mathbf{K}\boldsymbol{r}_{ij} = F_i, \quad (1)$$

where $\mathbf{M}$ is the mass-matrix containing the masses and moments of inertia of the particles, $\boldsymbol{r}_i$ and $\dot{\boldsymbol{r}}_i$ are the position and velocity vectors of particle i, $\boldsymbol{r}_{ij}$ and $\dot{\boldsymbol{r}}_{ij}$ are the corresponding relative position vectors for particles i and j, $\mathbf{C}$ and $\mathbf{C}'$ are damping matrices containing damping coefficient for drag and inelastic collisions, γ_{ij} is zero for particles not in contact and unity for particles in contact, γ'_{ij} is unity for connected particles and zero otherwise. $\mathbf{K}$ is the stiffness matrix and F_i is the sum of other forces acting on particle i. These forces may include gravitation, bouyancy, atmospheric and hydrodynamic/static forces, etc. In order to simulate ice (Schulson, 1999) we use the Young's modulus $E = 10^9\,\mathrm{N\,m^{-2}}$, density $\rho = 10^3\,\mathrm{kg\,m^{-3}}$ and fracture strain $\epsilon_c = (1\text{–}5) \times 10^{-4}$. The damping coefficient for collisions is $C' = 10^5\,\mathrm{N\,s\,m^{-1}}$. C represents the drag force on ice falling into water in a calving event, and is proportional to $|\dot{r}_i|$. If the contacts between the particles are broken, the material consisting of only the particles behaves as a fluid and the Poisson ratio is then $\nu \approx 0.5$. If the contacts are not broken, the material consisting of particles and beams, under small tensile deformations, deforms with $\nu \approx 0.3$.

In granular flow, the viscosity depends on e.g. the packing density and the cohesion between particles in contact. These are the two parameters that the most affect the diffusion of particles past each other, which is the microscopic origin of viscosity

TCD
7, 921–941, 2013

in any material. Viscosity of polycrystalline ice has similar microscopic mechanisms. One of the many contributions to viscosity of ice comes form grain-boundary sliding (Johari et al., 1995). In general, diffusion increases with temperature, which means more "liquid-like" for higher temperatures and more "solid-like" for lower temperatures. For ice, it therefore seems reasonable to model the viscous cohesion as a "melting-refreezing probability". This means that once the elastic beam that models the frozen contact between adjacent particles is stretched or bent, the probability for that beam to break becomes non-zero. In contrast, if the tensile strain of the beam reaches the fracture strain the contact always breaks. Also, when particles without a connecting beam are close to each other, a beam can be created with a small probability allowing the material to "refreeze". When combined, the two effects allow the material to undergo constant liquid-like deformation as well as fracture.

Furthermore, the melting-freezing probability can be adjusted to produce stress-dependent viscous flow obeying Glen's law for flow rate, $\xi = A\sigma^3$, where A is a temperature dependent Arrhenius factor and σ is stress. In more quantitative terms, we assume that melting events are random and uncorrelated with a probability $P = 1 - e^{-\lambda \Delta t}$ of melting a beam during a timestep Δt, where λ is the rate of melting. This implies that the flow rate of the simulated material is $\xi \approx \frac{\sigma}{E}\lambda$. By choosing $\lambda = 2A\frac{U}{a^2}E^2 \approx A\sigma^2 E$ we obtain Glen's law $\xi = A\sigma^3$. Here U is the elastic energy of the beam and a is the diameter of the discrete particles (equals the spacing of the simulation lattice). Correspondingly, dynamic viscosity is $\mu = \frac{\sigma}{\xi} \approx \frac{E}{\lambda} \approx \frac{1}{A\sigma^2}$.

The probabilities can be adjusted so that the desired viscosity can be acquired. Computational problems arise, however, from the fact that the time step length is limited by the rapid calving events to approximately 10^{-4} s, while the relevant time scale for viscous flow of ice is much longer. It is however possible to use lower viscosities and higher strain rates and re-scale the simulation time to match the ice behaviour as long as the viscous flow remain slow compared to all calving events. This approach is somewhat similar to the plasticity model used by Timar et al. (2010). Another, more simple, approach to imitate viscous behaviour is to use a weak and short-range attraction force

TCD
7, 921–941, 2013

for particles that are close to being in contact. This approach is more similar to the cohesion models of wet granular materials. Both approaches seem to give fairly realistic results. The former approach is benchmarked against a continuum model below.

3 Results

Figure 2 shows snapshots of a calving ice-block. The size of the block is 30 m × 30 m. The model block rests on a soft substrate that hinders the block from sliding. This "muddy sea floor" is modelled as a linear spring force prohibiting the block from sinking too deep and from moving sideways once it is stuck in the mud. The block is immersed in 20 m of water. The water is here modelled only as a buoyancy force. The simulation times of the snapshots are indicated. The time resolution in the simulation is 10^{-4} s. In this case the starting configuration is unstable and as soon as the simulation starts at time $t = 0$, cracks appear and the ice-block calves. The duration of this single calving event is 10–20 s, which is realistic in comparison with similar events in nature.

Figure 3 shows the fragment size distribution from the simulations displayed in Fig. 2. Results for three different simulations are shown and we distinguish between the size distributions early during the calving event and late during this process when the fragments have come to rest floating on the water. The fragment size distributions are compared with that of the universal crack-branching-merging model for fragmentation of brittle materials. This distribution is given by (Åström et al., 2004; Åström, 2006; Kekäläinen et al., 2007):

$$n(s) \propto s^{-(2D-1)/D} \exp(-s/s_0), \tag{2}$$

where s is the fragment or iceberg size or mass, D is the dimension ($D = 2$ for the simulations here and $D = 3$ for real glaciers), s_0 is a parameter which depends on, e.g. the material and the fracture energy. The result shown in Fig. 2 is consistent with field data by Crocker (1993) and Savage et al. (2000) from Bonavista Bay on Newfoundland, and with the data of Dowdeswell and Forsberg (1992) from Kongsfjorden on Svalbard.

TCD
7, 921–941, 2013

In order to verify the flow behaviour of the model a comparison with Elmer/Ice (Gagliardini and Zwinger, 2008; Zwinger and Moore, 2009) was made. In both simulations an ice block was placed on a flat surface with little/no friction and gravity as the only driving force. The result is displayed in Fig. 4. The deformation of the ice blocks are obviously quite similar. The main difference appears during the early times of the simulations. This is probably due to a partial jamming effect of the granular material. In the particle model the strain rate is roughly 10^5 times faster, which matches approximately the viscosity difference of the two models, i.e. strain rate is proportional to the inverse of viscosity. In a set of separate shear test with varying shear rates we also verified that the particle model can reproduce Glen's flow law to a high accuracy.

In order to further investigate the behaviour of our model we simulated the dynamics of an ice-block on a slope. We chose a block of size $200\,\mathrm{m} \times 50\,\mathrm{m}$ on a 18° slope ($\pi/10$). Again, the viscosity was roughly 10^5 lower than realistic values for ice, i.e. the Arrhenius factor $\approx 5 \times 10^{-19}\,\mathrm{s}^{-1}\,\mathrm{Pa}^{-3}$. We would thus expect that the strain rates will be roughly 10^5 higher than realistic rates for ice deformation. It is thus, in a crude sense, possible to re-scale the simulation time, which is calculated in seconds, to approximately days ($24\,\mathrm{h} = 0.864 \times 10^5\,\mathrm{s}$).

In order to further improve the simulations, we also introduced the possibility to locally switch between a high friction and zero friction for the contact between the substrate and the ice-block. We anchored the base of the block, indicated by a red line in Figs. 5 and 6, by high friction against the substrate. We also introduced a pressure, corresponding to the over-burden pressure on the upper vertical edge of the ice-block (Figs. 5 and 6). This simulates roughly the pressure induced by a slab of ice with same thickness upstreams. Finally, we investigate how the ice-block slides down-slope as a function of the fraction of the rest of the glacier being anchored to the substrate.

Figure 5 displays the case when only the top part of the ice-block is anchored. The rest is free to slide down-slope without friction. It is evident from this figure that the anchored part is not enough to keep the ice-block in place. It breaks near the substrate and the entire block slides down-slope. If the time is re-scaled as explained above, the velocity reaches roughly 5 m/day, which is comparable to observed rates (about 10–100 m d^{-1}, Cuffey and Paterson, 2010) for surging glaciers.

In the opposite limit, when there are additional frictional anchoring points on the lower part of the slope, the ice-block cannot move, but is stuck. In this case only a smaller part of the block, near the lower edge, calves, fragments and flows a limited distance down the slope. As this layer of highly fragmented ice flows, it gets thinner and the force driving it down-hill decreases and it slows down. This is displayed in Fig. 6.

In order to quantify the above, Fig. 7 shows kinetic energy (E_{kin}) as a function of time for varying amounts of frictional contact on the lower slope as described for Figs. 5 and 6. The various lines in Fig. 7 correspond to two different phases, a surging phase, when the entire ice-block slides down the slope, and a quiescent phase, when only part of the front of the ice-block fractures and flows down-hill. For some of the simulated cases there appears to be a phase-transition during the simulation run time. In these cases the kinetic energy is initially in the quiescent phase and at some point in time the kinetic energy suddenly increases and rapidly approaches that of the surging phase. Sometimes surging does not appear for the entire block, and the kinetic energy only increases part-way towards the surging phase before stabilizing.

Finally, to highlight the difference between the single calving event represented by Fig. 2, and the surging glaciers in Fig. 5, the fragment size distribution was calculated for the surging glacier simulation (Fig. 3). In this case the fragment size distribution was equivalent to that usually found for a grinding process (Åström, 2006).

4 Discussion

The new model we introduced present in this paper is certainly not feasible to incorporate into ice sheet models given the extensive computing power required. It may however be used to investigate details of calving processes and relationships such as dependence of crevassing rate and fragment size on water depth, or the presence and influence of water on fracture processes. The model also has considerable potential to test and improve parameterizations of fracturing and calving used in continuum models. The resolution of many models simply does not include small ice-cliff failure, and, since calving and fracturing are essentially discontinuous processes, introducing them into continuum models is problematic. Cuffey and Paterson (2010) summarized the situation as: most models either let ice shelves advance to the edges of the model grid, or assume that ice shelves terminate at a prescribed water depth (400 m typically). For marine-terminating glaciers that are not fully floating, most models either assume that calving rate increases with water depth, or constrain the ice front thickness instead of the calving rate. However recent progress has been considerable in the field of parameterizing crevassing by weakening the ice rheology in a damage model.

Our discrete particle formulation may be seen as a complementary method to statistical continuum damage approaches that have been applied to ice shelves (e.g. Borstad et al., 2012) or to mountain glacier calving (e.g. Jouvet et al., 2011). This can be illustrated by, for example, Levermann et al. (2012) who formulated the vertically averaged ice strain rate tensor, which can be determined from the spatial derivative of the remotely sensed velocity pattern. His model can then be tuned to observations of specific ice shelves, and no other observations are needed for the model to "carry itself forward" into the future. That is, it can "predict" calving without any other observation inputs (the necessary inputs would all come from the dynamic ice sheet model). Over broad areas of an ice shelf, the viscosity is reduced by crevasses (e.g. along the flow units coming from different tributary ice streams and glaciers), or the ice may be strengthened by the presence of sub ice shelf freeze-on of ocean water. The crevasses can be readily seen in imagery, and these images can be used to tune models for ice viscosity and fracture initiation stress in specific ice shelves or tributary ice streams to give similar patterns of both crevassing and velocities as observations (Albrecht and Levermann, 2012a,b).

Above we demonstrated the importance of basal friction to the behaviour of the particle model. Fast outlet ice streams and surging glaciers are governed by the physics of basal sliding. In temperate glaciers (i.e. glaciers with temperatures at the pressure melting point) sliding behaviour is often tightly interlinked with basal hydrology. On the continental ice sheets, the fast flowing ice streams, and outlet glaciers owe their speed to basal sliding in addition to internal ice deformation. Schoof (2009) showed that a variety of friction laws converged on the Coulomb friction law in appropriate parametric limits which can usefully describe a plastic till rheology. The motion of ice streams appears to depend critically on the distribution and nature of regions of high drag ("sticky spots", Alley, 1993). It is not known what controls the present configuration of these features, though presumably they are related to the bed roughness and geometry either directly as a bedrock bump, or by routing water supply and till properties. Inverse methods can be used to determine the spatial variability of basal friction (Raymond and Gudmundsson, 2009; Morlighem et al., 2010; Petra et al., 2012; Arthern and Gudmundsson, 2010; Jay-Allemand et al., 2011; Schäfer et al., 2012), in an analogous way to the damage weakening of shear margins and crevasse damage on ice shelves.

The discrete particle model we use here clearly suffers from lack of three dimensional geometry; hence it is presently limited to the testing or verification of the parameterization used in continuum models. It is plausible to incorporate basal friction laws that could mimic more accurately a plastic basal till with sticky spots. Our model prediction for the particle size distributions can be readily tested in observational data on surface crevassing and iceberg calving.

Acknowledgements. This publication is contribution number 22 of the Nordic Centre of Excellence SVALI, "Stability and Variations of Arctic Land Ice", funded by the Nordic Top-level Research Initiative (TRI). The work has been supported by the SVALI project through the University of Lapland, Arctic Centre, and through the University Centre in Svalbard. The funding is gratefully acknowledged.

References

Albrecht, T. and Levermann, A.: Fracture-induced softening for large-scale ice dynamics, EGU General Assembly, Vienna, Austria, 22–27 April, 2012a. 930

Albrecht, T. and Levermann, A.: Fracture field for large-scale ice dynamics, J. Glaciol., 58, 165–176, doi:10.3189/2012JoG11J191, 2012b. 930

Alley, R. B.: In search of ice-stream sticky spots, J. Glaciol., 39, 447–454, 1993. 931
Arthern, R. J. and Gudmundsson, G. H.: Initialization of ice-sheet forecasts viewed as an inverse Robin problem, J. Glaciol., 56, 527–533, 2010. 931
Åström, J. A.: Statistical models of brittle fragmentation, Adv. Phys., 55, 247–278, 2006. 927, 929
Åström, J. A., Ouchterlony, F., Linna, R. P., and Timonen, J.: Universal dynamic fragmentation in D dimensions, Phys. Rev. Lett., 92, 245506, doi:10.1103/PhysRevLett.92.245506, 2004. 927
Bassis, J. N.: The statistical physics of iceberg calving and the emergence of universal calving laws, J. Glaciol, 57, 3–16, 2011. 923
Benn, D. I., Hulton, N. R. J., and Mottram, R. H.: “Calving laws”, “sliding laws” and the stability of tidewater glaciers, Ann. Glaciol., 46, 123–130, 2007a. 923
Benn, D. I., Warren, C. R., and Mottram, R. H.: Calving processes and the dynamics of calving glaciers, Earth Sci. Rev., 82, 143–179, 2007b. 923
Borstad, C. P., Khazendar, A., Larour, E., Morlighem, M., Rignot, E., Schodlok, M. P., and Seroussi, H.: A damage mechanics assessment of the Larsen B ice shelf prior to collapse: towards a physically based calving law, Geophys. Res. Lett., 39, L18502, doi:10.1029/2012GL053317, 2012. 923, 930
Burgess, D. O., Sharp, M. J., Mair, D. W. F., Dowdeswell, J. A., and Benham, T. J.: Flow dynamics and iceberg calving rates of Devon Ice Cap, Nunavut, Canada, J. Glaciol., 51, 219–230, 2005. 923
Crocker, G. B.: Size distributions of bergy bits and growlers calved from deteriorating icebergs, Cold. Reg. Sci. Technol., 22, 113–119, 1993. 927
Cuffey, K. M. and Paterson, W. S. B.: The Physics of Glaciers, 4 Edn., Academic Press, 704, 2010. 929, 930
Dowdeswell, J. A. and Forsberg, J. A.: The size and frequency of icebergs and bergy bits derived from tidewater glaciers in Kongsfjorden, northwest Spitsbergen, Polar Res., 11, 81–91, 1992. 927
Dowdeswell, J. A., Benham, T. J., Strozzi, T., and Hagen, J. O.: Iceberg calving flux and mass balance of the Austfonna ice cap on Nordaustlandet, Svalbard, J. Geophys. Res., 113, F03022, doi:10.1029/2007JF000905, 2008. 923
Gagliardini, O. and Zwinger, T.: The ISMIP-HOM benchmark experiments performed using the Finite-Element code Elmer, The Cryosphere, 2, 67–76, doi:10.5194/tc-2-67-2008, 2008. 928

TCD
7, 921–941, 2013

A particle based simulation model for glacier dynamics

J. A. Åström et al.

Jacob, T., Wahr, J., Pfeffer, W. T., and Swenson, S.: Recent contributions of glaciers and ice caps to sea level rise, Nature, 482, 514–518, doi:10.1038/nature10847, 2012. 923

Jay-Allemand, M., Gillet-Chaulet, F., Gagliardini, O., and Nodet, M.: Investigating changes in basal conditions of Variegated Glacier prior to and during its 1982–1983 surge, The Cryosphere, 5, 659–672, doi:10.5194/tc-5-659-2011, 2011. 931

Johari, G. P., Pascheto, W., and Jones, S. J.: Anelasticity and grain boundary relaxation of ice at high temperatures, J. Phys. D Appl. Phys., 28, 112, doi:10.1088/0022-3727/28/1/018, 1995. 926

Jouvet, G. and Rappaz, J.: Analysis and finite element approximation of a nonlinear stationary Stokes problem arising in glaciology, Adv. Numer. Anal., doi:10.1155/2011/164581, 2011.

Jouvet, G., Picasso, M., Rappaz, J., Huss, M., and Funk, M.: Modelling and numerical simulation of the dynamics of glaciers including local damage effects, Math. Model. Nat. Phenom., 6, 263–280, doi:10.1051/mmnp/20116510, 2011. 923, 930

Kekäläinen, P., Åström, J. A., and Timonen, J.: Solution for the fragment-size distribution in crack-branching model of fragmentation, Phys. Rev. E, 76, 026112, doi:10.1103/PhysRevE.76.026112, 2007. 927

Levermann, A., Albrecht, T., Winkelmann, R., Martin, M. A., Haseloff, M., and Joughin, I.: Kinematic first-order calving law implies potential for abrupt ice-shelf retreat, The Cryosphere, 6, 273–286, doi:10.5194/tc-6-273-2012, 2012. 923, 930

Morlighem, M., Rignot, E., Seroussi, H., Larour, E., Dhia, H. B., and Aubry, D.: Spatial patterns of basal drag inferred using control methods from a full-Stokes and simpler models for Pine Island Glacier, West Antarctica, Geophys. Res. Lett., 37, L14502, doi:10.1029/2006JF000576, 2010. 931

Nick, F. M., van der Veen, C. J., Vieli, A., and Benn, D. I.: A physically based calving model applied to marine outlet glaciers and implications for their dynamics, J. Glaciol., 56, 781–794, 2010. 923, 924

Petra, N., Zhu H., Stadler, G., Hughes, T. J. R., and Ghattas, O.: An inexact Gauss–Newton method for inversion of basal sliding and rheology parameters in a nonlinear Stokes ice sheet model, J. Glaciol., 58, 889–903, 2012. 931

Raymond, M. J. and Gudmundsson, G. H.: Estimating basal properties of ice streams from surface measurements: a non-linear Bayesian inverse approach applied to synthetic data, The Cryosphere, 3, 265–278, doi:10.5194/tc-3-265-2009, 2009. 931

Rignot, E., Mouginot, J., and Scheuchl, B.: Ice flow of the Antarctic ice sheet, Science, 333, 1427–1430, doi:10.1126/science.1208336, 2011. 923

Savage, S. B., Crocker, G. B., Sayed, M., and Carriers, T.: Cold. Reg. Sci. Technol., 31, 163–172, 2000. 927

Schoof, C.: Coulomb friction and other sliding laws in a higher order glacier flow model, Math. Model. Meth. Appl. Sci., 20, 157–189, 2009. 931

Schulson, E. M.: The structure and mechanical behavior of ice, JOM, 51, 21–27, 1999. 925

Schäfer, M., Zwinger, T., Christoffersen, P., Gillet-Chaulet, F., Laakso, K., Pettersson, R., Pohjola, V. A., Strozzi, T., and Moore, J. C.: Sensitivity of basal conditions in an inverse model: Vestfonna ice cap, Nordaustlandet/Svalbard, The Cryosphere, 6, 771–783, doi:10.5194/tc-6-771-2012, 2012. 931

Thomas, R. H., Rignot, E. J., Kanagaratnam, K., Krabill, W. B., and Casassa, G.: Force-perturbation analysis of Pine Island Glacier, Antarctica, suggests cause for recent acceleration, Ann. Glaciol., 39, 133–138, doi:10.3189/172756404781814429, 2004. 923

Timar, G., Blomer, J., Kun, F., and Herrmann, H. J.: New universality class for the fragmentation of plastic materials, Phys. Rev. Lett., 104, 095502, doi:10.1103/PhysRevLett.104.095502, 2010. 926

Vieli, A., Payne, A. J., Du, A., and Shepherd, A.: Numerical modeling and data assimilation of Larsen B ice shelf, Antarctic Peninsula, Philos. T. Roy. Soc. A, 364, 1815–1839, 2006. 923

Walter, F., O'Neel, S., McNamara, D., Pfeffer, W. T., Bassis, J. N., and Fricker, H. A.: Iceberg calving during transition from grounded to floating ice: Columbia Glacier, Alaska, Geophys. Res. Lett., 37, L15501, doi:10.1029/2010GL043201, 2010. 923

Zwinger, T. and Moore, J. C.: Diagnostic and prognostic simulations with a full Stokes model accounting for superimposed ice of Midtre Lovénbreen, Svalbard, The Cryosphere, 3, 217–229, doi:10.5194/tc-3-217-2009, 2009. 928

TCD

7, 921–941, 2013

A particle based simulation model for glacier dynamics

J. A. Åström et al.

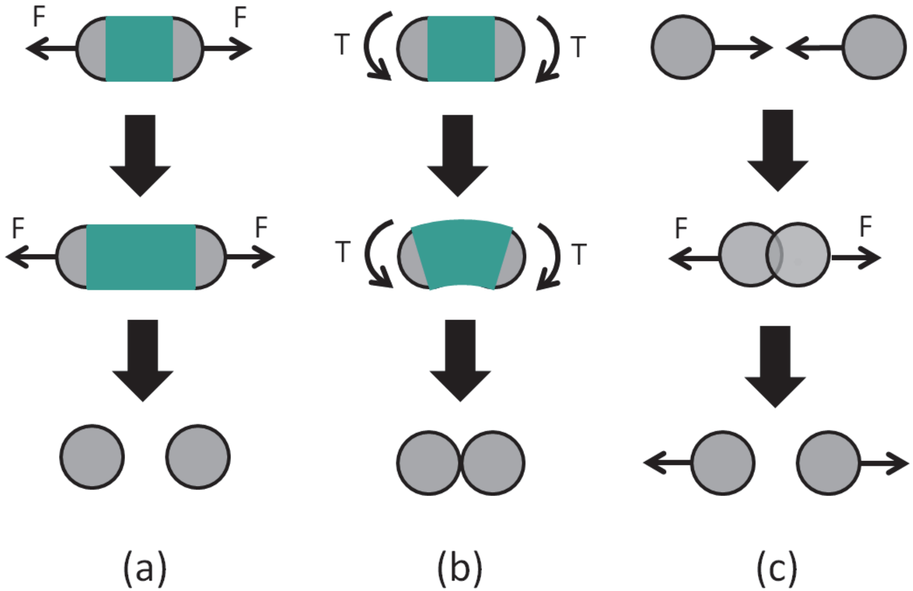

Fig. 1. The particles connected with a beam can **(a)** stretch when a force F is applied and **(b)** bend when a torque T is applied. Particles that overlap, i.e. come into contact **(c)** will experience repulsive forces. The amount of stretching and bending required for beam breaking is highly exaggerated as is the amount of overlapping of the particles occuring in the simulations.

TCD
7, 921–941, 2013

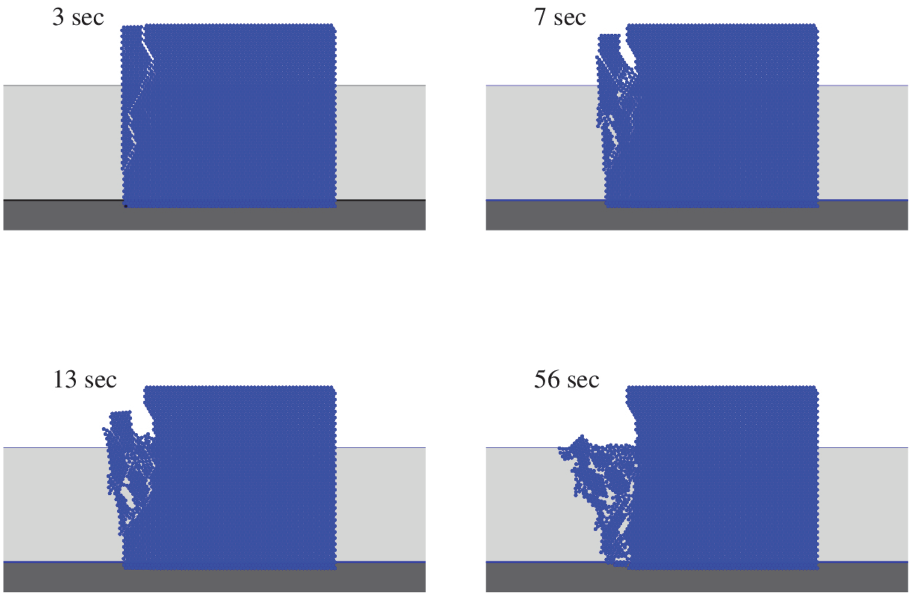

Fig. 2. Snapshots of a calving ice-block. The size of the block is 30 m × 30 m. The block rests on a soft substrate that efficiently hinders the block from sliding, thus modellling e.g. a muddy sea floor. The block is immersed in 20 m of water. The simulation times of the snapshots are indicated.

TCD
7, 921–941, 2013

A particle based simulation model for glacier dynamics

J. A. Åström et al.

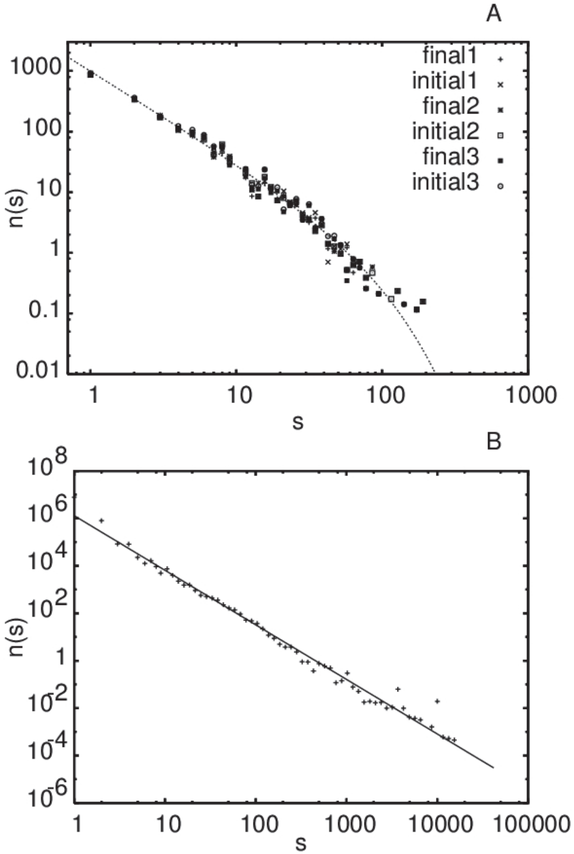

Fig. 3. (A) The fragment size distribution for simulations like the one in Fig. 2. The figure displays the results for three different simulations and both the distribution early during the calving event and later when the fragments have come to rest floating on the water. The line is the distribution predicted from Eq. (2). **(B)** The fragment size distribution $n(s)$ for a surging glacier. In this case $n(s) \propto s^{-2.3}$.

TCD
7, 921–941, 2013

A particle based simulation model for glacier dynamics

J. A. Åström et al.

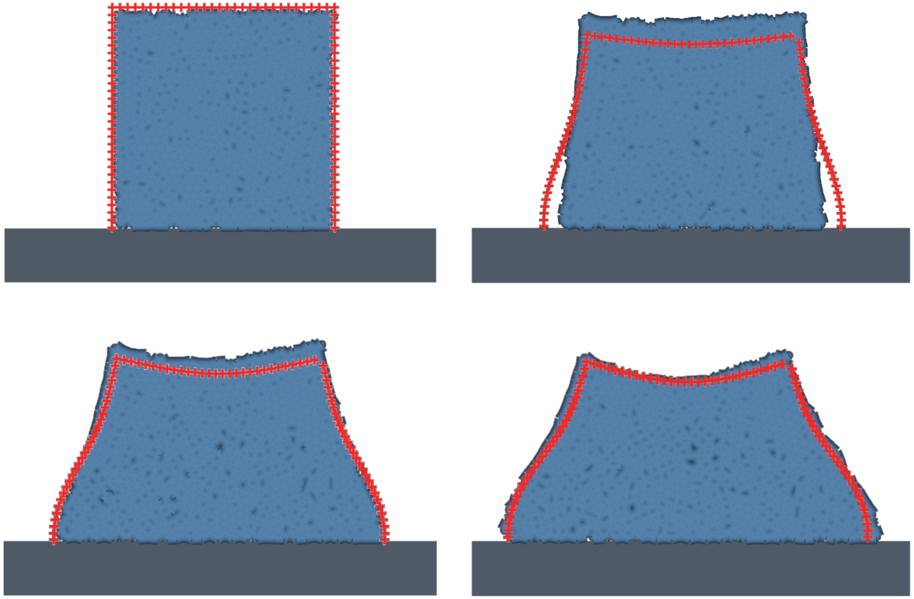

Fig. 4. Snapshots of a deforming ice block simulated with Elmer/Ice and our particle model. In the Elmer/Ice simulation (red markers) the snapshots are from timesteps 0, 3, 5 and 7 yr and the particle model snapshots (blue area) are from corresponding time steps. The size of the block is 30 m × 30 m and the time span of the Elmer/Ice simulation is roughly 10^8 s compared to the 10^3 s time span of the particle simulation.

TCD
7, 921–941, 2013

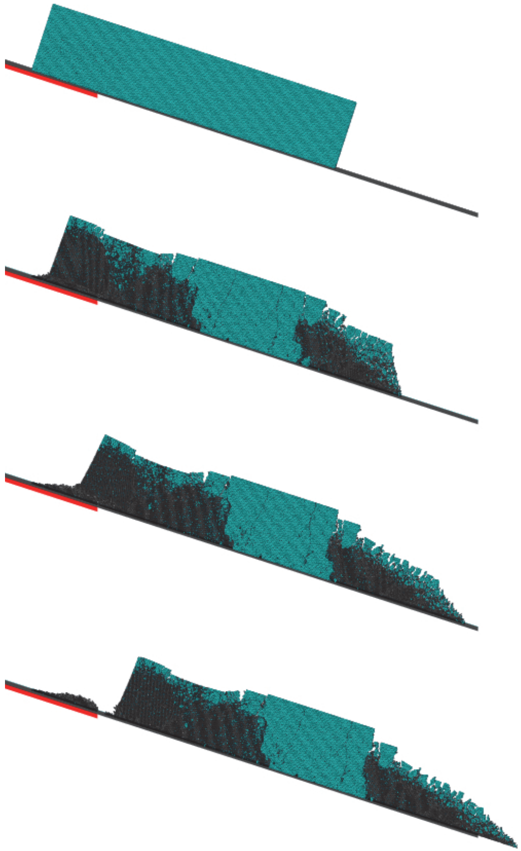

Fig. 5. Snapshots of a 200 m × 50 m ice-block on a 18° slope. The red line marks a high friction contact. The colors of the ice-block represent elastic areas where the elastic beams between particles have not been broken (green) and viscous areas where beams are no longer intact (gray). The pressure of upstream ice slab on the slope above the ice-block is not shown in the figure.

TCD
7, 921–941, 2013

A particle based simulation model for glacier dynamics

J. A. Åström et al.

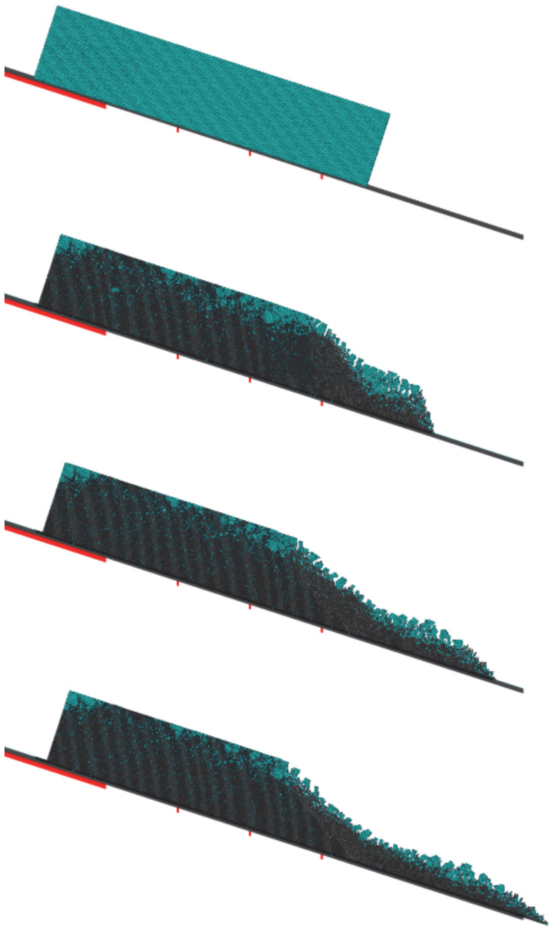

Fig. 6. Similar as in Fig. 5, but with several "frictional anchors", indicated by red markers, also on the lower part of the slope.

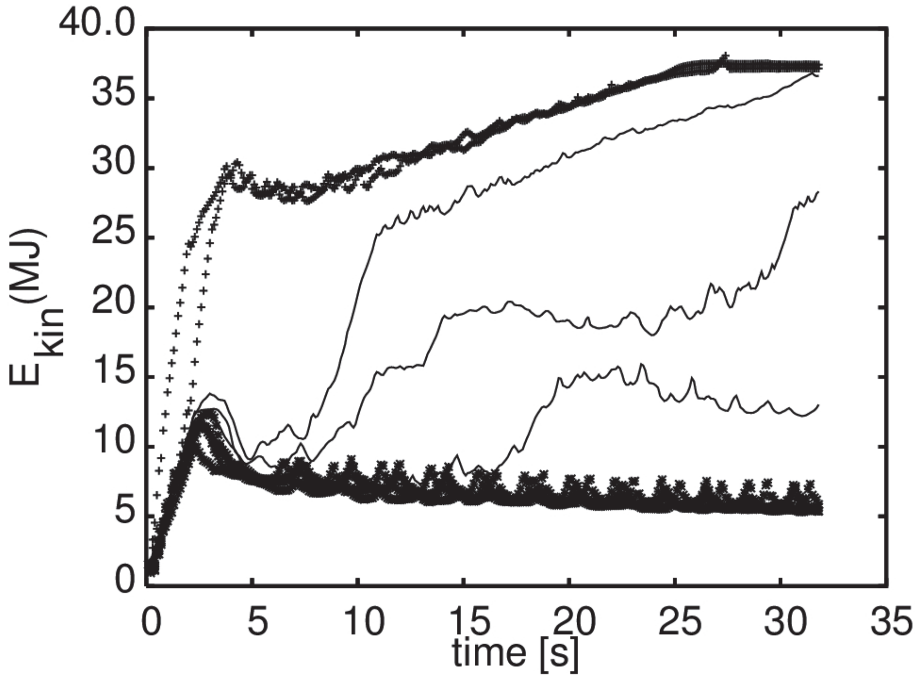

Fig. 7. The kinetic energy (E_{kin}) as function of time for "surging" simulations exemplified by Figs. 5 and 6. The cases when the ice-block is the entire time in either the surging or the quiessent phase the energy is indicated by markers. For the blocks for which a phase transition appear, the kinetic energy is represented by lines.

TCD
7, 921–941, 2013

A particle based simulation model for glacier dynamics

J. A. Åström et al.